Application of GNSS-supported static terrestrial lidar in mapping landslide processes in the Himalaya

Megotsohe Chasie*, P. K. Theophilus, Akshaya Kumar Mishra, Saibal Ghosh and Shib Kanta Das

Geohazards Research and Management Centre, Geological Survey of India, Kolkata 700 091, India

Site-specific topographic survey of 15 landslides in the four mountainous states of India, namely Uttarakhand, Jammu & Kashmir, Sikkim and Nagaland, was carried out through a terrestrial laser scanner campaign. The versatility of the lidar instrument in topographic surveys and its advantages over conventional survey practices are highlighted. The effective use of the static terrestrial lidar in the rapid characterization and hazard assessment of landslides in this study is presented for adoption as a meaningful hazard assessment strategy in the hilly terrains.

Keywords: Hazard assessment, hilly terrain, landslide, terrestrial lidar, topographic survey.

THE basic requirement for any site-specific landslide analysis is the availability of a topographic basemap of suitable accuracy at the desired scale. It enables mapping, plotting and representing all geological and non-geological features on the slope under study. Often, the primary predicament lies in the availability or time-bound generation of basemaps for such large-scale studies. In the Indian context, conventional survey methods using total station (TS) instruments to generate basemaps are common, particularly for large-scale studies. However, such surveys are time-consuming and labour-intensive in terms of data acquisition, often compelling the operator to set-up and work from several datums[1]. Further, the presence of unfavourable site conditions like vegetation cover can lead to acquisition of less data points, thereby flattening subtle topographic features that may be crucial for accurate characterization of the slope[2].

The rapid development of light detection and ranging (lidar) technology, a three-dimensional remote sensing technique, during the past two decades has drastically improved the way we perceive and model the earth's surface processes[3–5]. In this technique, the earth's surface is scanned by laser scanners mounted over fixed or mobile platforms, including drones/unmanned aerial vehicles (UAVs), helicopters, etc. to enable quick, 3D data capturing based on the project requirements. The terrestrial laser scanner (TLS) is one such ground-based survey instrument working on lidar technology, where a laser beam (pulse or continuous wave) is transmitted onto a surface and the returning signal is recorded for distance measurement. TLS can be fixed/mounted on a tripod, in which case the platform is static/stationary, or can be vehicle-mounted for a dynamic/moving platform. This relief imaging by the scanner is used to extract very accurate digital elevation models (DEMs). A DEM is the digital representation of the topography/land surface elevation with respect to a given reference datum. During the last two decades, the use of DEM and its derivatives for determining terrain or morphometric attributes (slope, aspect, curvature, elevation, etc.) has provided more efficient ways for detailed landscape studies of landslides[6–10]. Acquisition of multi-temporal datasets through repeated laser scanning has been exploited by various workers for producing a DEM of difference (DoD) that allows for quantification of volumes and ground displacement changes[9,11–15], and for monitoring of slopes[16–18]. Targeted laser scanning on exposed rock slopes to characterize rock discontinuities has also been carried out[19–23].

However, the potential of the technology and utility of the TLS output data, i.e. the 3D point cloud, the high-resolution digital elevation model (HRDEM) and its derivative products in landslide studies are yet to be fully exercised/adopted in a country like India, having 12.6% of its land mass (about 0.42 million km^2) susceptible to landslides (www.gsi.gov.in/webcenter/portal/OCBIS/pageGeoInfo/pageLANDSLIDEHAZRD?). Since the use of lidar-derived datasets in detailed landslide studies is still in the evolving stage, this study showcases the benefits of the technology and versatility of the static terrestrial lidar instrument in site-specific topographic surveys for maximum exploitation of the state-of-the-art devices by the Indian geoscientific community.

Study sites and nature of work

Site-specific topographic surveys using the ground-based static lidar were carried out for 15 landslides distributed in four mountainous states of India, namely Uttarakhand, Jammu & Kashmir (J&K), Sikkim and Nagaland (Figure 1), where the first three states are physiographically located

*For correspondence. (e-mail: megochasie@gmail.com)

well within the rugged Himalayan domain and the fourth state is in the sub-Himalayan domain. Studies in Uttarakhand involved rapid geological assessment of two sites, one at Devprayag on the right bank slope of Bhagirathi River (during February 2019) and the other for relocation of a part of Bhatwari village affected by landslides (during November 2019). The site in Nagaland was chosen for rapid assessment of the infamous Phesama landslide known for repeated closure of the strategic National Highway-29 to Imphal. The studies in J&K included 11 landslide sites along the Batote–Ramban–Banihal sector of NH-44 connecting Jammu and Srinagar townships, initiated mainly due to recent road-widening activities. The large number of sites requiring immediate attention to stabilize the slopes along this strategic road were assessed during October–November 2020 on priority before the onset of the next monsoon. In Sikkim, an assessment of a landslide affecting the Rangpo–Rorathang road corridor (at the 3rd Mile) as well the premises of a pharmaceutical company was completed in January 2021. The elevation of all the study sites ranged from 334 m amsl (at the 3rd Mile landslide, Sikkim) to a maximum of 1948 m amsl (at Kharpora landslide, J&K) and may be considered low elevation when viewed from the Himalayan perspective. Owing to the lower elevation, most of the test sites bear significant vegetation cover.

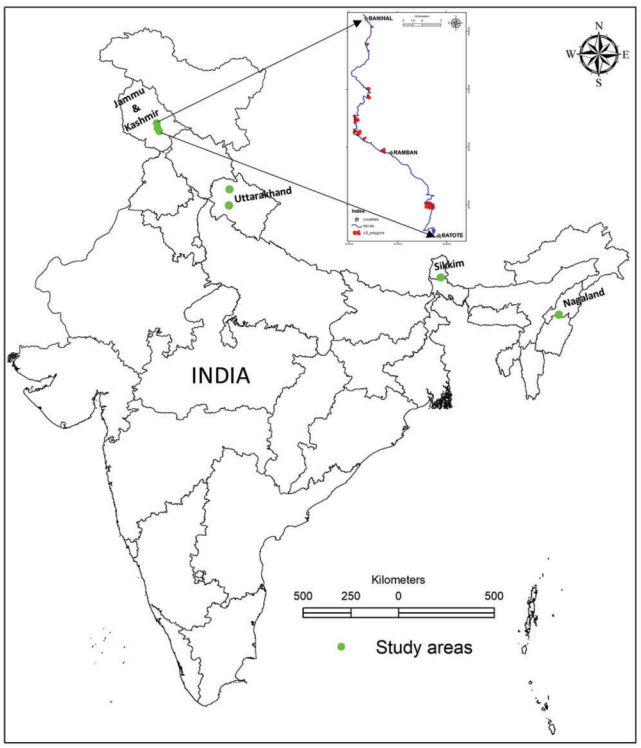

Figure 1. Location of the study areas. India map after Survey of India[42]. The 11 sites along Batote–Ramban–Banihal sector of NH-44, Jammu & Kashmir (J&K) are enlarged.

Methodology

TLS measurement principle and instrument used:

Range determination or distance measurement by laser scanners is primarily carried out in two ways: the phase and pulse methods[24]. While the phase-based scanners are more accurate, they suffer from a limited range. On the other hand, pulse-based (also time-of-flight) scanners are implemented in most TLS as they offer a longer effective measurement range[24,25]. The measurement principle in a TLS involves the emission of many short infrared or laser light pulses to a target surface. In the process, the emitted laser pulses may get reflected from various objects in their path/line-of-sight such as birds, vegetation, man-made obstructions, ground surface, etc., leading to several backscattered pulses (echoes) from one emitted pulse. The precise time stamp for each returning light pulse (round trip) is determined directly by the scanner. With the velocity of light through a medium known, the distance between the scanner and target is determined by $D = c*\Delta t/2$, where c is the speed of light and Δt is the round-trip travel time. For determination of position XYZ relative to the scanner, rotating/oscillating mirrors are used to deflect the laser pulse in a direction well-defined to the scanner's orientation (roll, pitch and yaw angles). Since the positions determined are relative the scanner, georeferencing of the point cloud is done for assigning coordinates in the global system, generally through the use of a set of ground control points (GCPs) whose precise coordinates are obtained through the Global Navigation Satellite System (GNSS). Based on the range and measurement rate of the instrument used, a large amount of 3D data can be acquired within a few minutes. This raw scan dataset in the order of several thousand points is termed a point cloud.

The laser scanner used in the project is the RIEGL VZ-4000, with a moderately long scanning range of 4000 m under 90% reflectivity conditions. The effective measurement rate of the instrument ranges from 23,000 measurements per second at 30 kHz laser pulse repetition rate to 222,000 measurements per second at 300 kHz laser pulse repetition rate. With a beam divergence rate of 0.15 mrad, the laser beam footprint measuring 18 mm at exit increases to 300 mm at 2000 m (ref. 26). Calibrated digital camera (both in-built and detachable external camera) for simultaneous filming of terrain along with scanning is provisioned for the capture of RGB data.

Terrestrial lidar workflow

A sequential workflow in the operational use of TLS can be generalized and grouped into four stages, each consisting of a series of steps (Figure 2). The planning and reconnoitary survey stage primarily is the development of an execution plan which includes preparation of the instrument

and accessories, site survey for accessibility conditions and selection of optimum scan position/s for complete coverage of the area-of-interest (AOI), selection of GCPs and estimation of suitable time for scanning. The rugged Himalayan terrain with complex slope morphometry often necessitates scanning from multiple viewpoints for minimal occlusion.

The data acquisition stage consists of GNSS data observation for establishing local control in positioning within the test site/s and scanner data acquisition. For GNSS data, a standalone base station is set up in a secure, open space for minimal multipath errors (Figure 3 *a*). Dual frequency (L1 and L2) data in static mode with sampling rate at 1 or 2 s intervals are acquired for ≥120 h to facilitate better point convergence through a longer observational period. Post-processing of the acquired data is then carried out for positioning accuracy. Prior to laser scanning, GCPs are identified in the vicinity of the proposed scan position and target reflectors are placed over the GCPs during scanning to enable target-based registration or georeferencing of the point cloud in the global coordinate system (Figure 3 *b*). A minimum of three GCPs/target reflectors are required for triangulation and registration of a single scan. For target-based registration of the point cloud in the global coordinate system, GNSS data observation over the identified GCPs in fast static mode (1 h duration) is carried out prior to or after scanning, the data observation being done simultaneously with that of the base station. The baselines are then processed using the established base station coordinates as reference.

Optimum scan positions, though always not feasible, are with a clear line-of-sight allowing maximum coverage of the AOI and located at normal or near orthogonal positions to the target surface. This allows for maintaining a nearly uniform linear distance to the target surface, which then allows for a low incidence angle that, in turn, allows better reflectivity and, therefore, a higher quality data acquisition. Before scanning, the scanner parameters are configured based on the site conditions and project deliverables. The desired resolution for data capturing, driven here by the scale of geological features to be measured, is a function of the laser beam divergence rate and the angular resolution (angle between two laser spots). Based on the estimated range to the target surfaces and scale of features to be mapped, an angular resolution of 0.02° has been adopted for all the sites in the present study. Challenges such as sudden changes in weather conditions (detrimental to photographic image acquisition), unexpected disruptions in the scanner or power supply, etc. may be encountered at this stage and dealt with appropriately. The result of the scanner data acquisition is a point cloud from a single scan or a fusion of point clouds from multiple scans having sufficient overlap areas (≈30%).

The data processing and post-processing stages, which involve data transformation and treatment of the point cloud, qualify as the most tedious and time-consuming segment of any terrestrial lidar project. In the present study, RIEGL's RiSCAN PRO software was used for all data transformation and treatment activities. The scan datasets from different viewpoints for each site were aligned and merged to develop a complete model. The alignment of multiple point clouds into a single, continuous point cloud was realized using prominent but common features between two adjacent scans. The multi-station adjusted point cloud was then georeferenced using the post-processed coordinates of relevant GCPs. For developing a 3D photorealistic model, colourization of the point cloud through the software-based allocation of the RGB value from the camera-captured image/raster was done. Next, the fully transformed raw point cloud was cleaned in two stages to optimize the data quality. In the first stage, the off-terrain points (e.g. vegetation, buildings, wires, moving objects such as vehicles, etc.) were separated from the terrain points using various terrain filters. An initial first-level removal of unwanted data/noise in the acquired point cloud using the echo of signals returning from the emitted surface is shown in Figure 4, enabling the generation of a bare earth model. The second

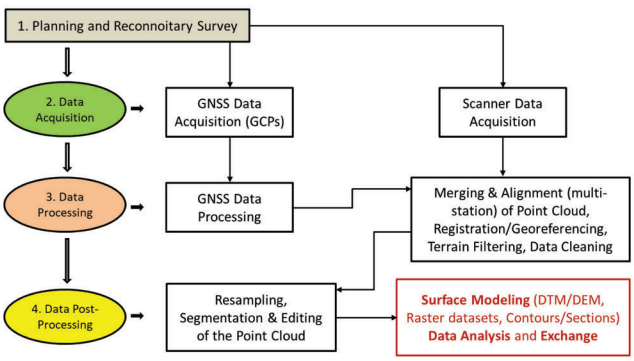

Figure 2. A generalized workflow in the operational use of terrestrial laser scanner.

Figure 3. Components of data acquisition. ***a***, GNSS base station set up on a rooftop at Phesama, Nagaland. ***b***, Field scanning conditions illustrating setting up of target reflectors.

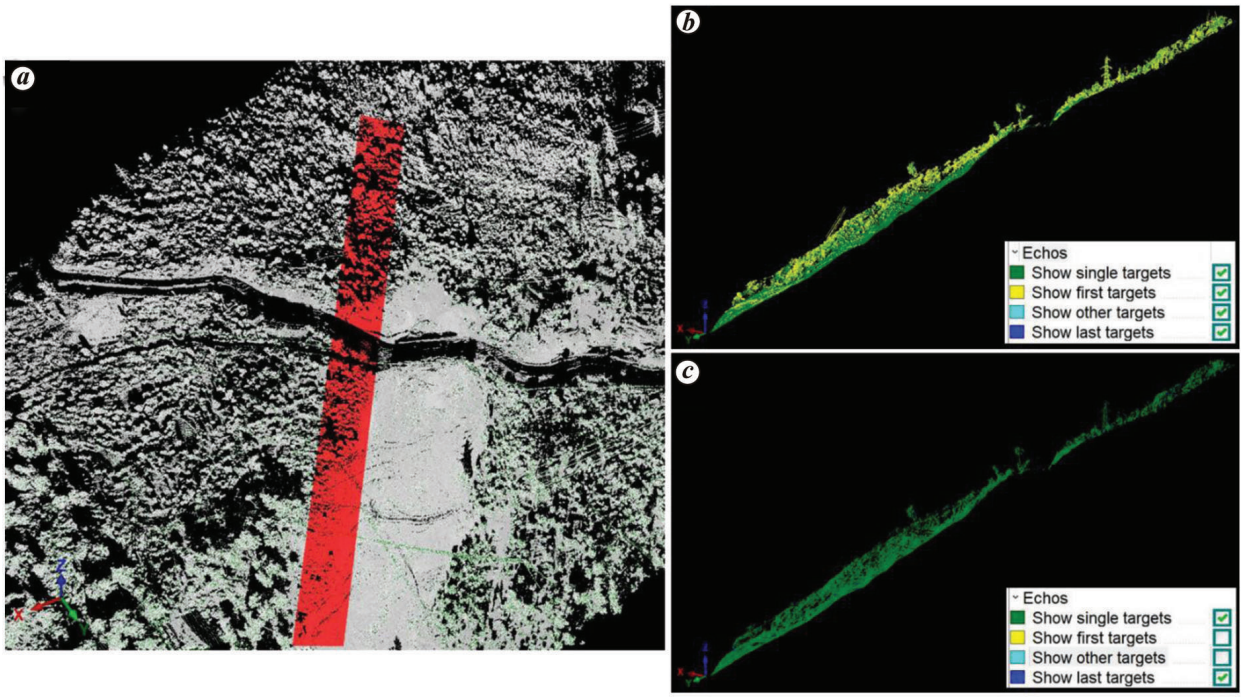

Figure 4. A first-level noise removal in the point cloud acquired for Peerah landslide, J&K. ***a***, The point cloud is presented in reflectance scale and a patch (in red) selected for controlled data treatment. ***b***, Lateral view of the selected patch showing segregation of the point cloud based on digitized echo signals (arrival time of backscattered pulses). ***c***, Removal of unwanted data/noise based on echo signals.

Table 1. Area versus timeframe for field data acquisition (TLS and GNSS)

Landslide/study area	Location	Area of HRDEM prepared (km^2)	Minimum time (h) required for field data acquisition (no. of scan positions × 1 h + no. of ground control points × 1 h)
3rd Mile	3rd Mile on Rangpo–Rorathang Road, Sikkim	0.47	(2 × 1 + 4 × 1) = 6
Bhatwari	Bhatwari village, Uttarakhand	0.94	(2 × 1 + 5 × 1) = 7
Devprayag	Devprayag village, Uttarakhand	1.10	(4 × 1 + 6 × 1) = 10
Chamalwas	Batote–Ramban–Banihal sector of NH-44, Jammu & Kashmir (J&K)	0.25	(1 × 1 + 4 × 1) = 5
Dalwas	Batote–Ramban–Banihal sector of NH-44, J&K	0.48	(2 × 1 + 4 × 1) = 6
Digdole	Batote–Ramban–Banihal sector of NH-44, J&K	0.82	(2 × 1 + 4 × 1) = 6
Kharpora	Batote–Ramban–Banihal sector of NH-44, J&K	0.13	(1 × 1 + 4 × 1) = 5
Marog1	Batote–Ramban–Banihal sector of NH-44, J&K	0.30	(2 × 1 + 4 × 1) = 6
Marog2	Batote–Ramban–Banihal sector of NH-44, J&K	0.61	(2 × 1 + 4 × 1) = 6
Monkey-more	Batote–Ramban–Banihal sector of NH-44, J&K	0.32	(1 × 1 + 4 × 1) = 5
Monpassi	Batote–Ramban–Banihal sector of NH-44, J&K	0.31	(2 × 1 + 4 × 1) = 6
Panthial	Batote–Ramban–Banihal sector of NH-44, J&K	0.34	(2 × 1 + 4 × 1) = 6
Peerah	Batote–Ramban–Banihal sector of NH-44, J&K	1.25	(4 × 1 + 6 × 1) = 10
Serri	Batote–Ramban–Banihal sector of NH-44, J&K	0.49	(2 × 1 + 5 × 1) = 7
Phesama	NH-29 at Phesama village, Nagaland	0.84	(4 × 1 + 6 × 1) = 10

stage involves manually cleaning and refining the data overlooked by the terrain filters that can give rise to false terrain. Depending on the project requirements, the refined point cloud may be resampled or segmented for improved feature identification/extraction. The DEM/digital terrain model (DTM) for the AOI was then generated using the refined point cloud (through rasterization or generating a mesh).

Advantages of terrestrial lidar in topographic surveys

Terrestrial lidar instruments provide high-resolution topographic data with notable advantages over conventional surveying techniques[27]. Among the many advantages of using a ground-based laser scanner for topographic surveys compared to TS is the quick turnaround of output data

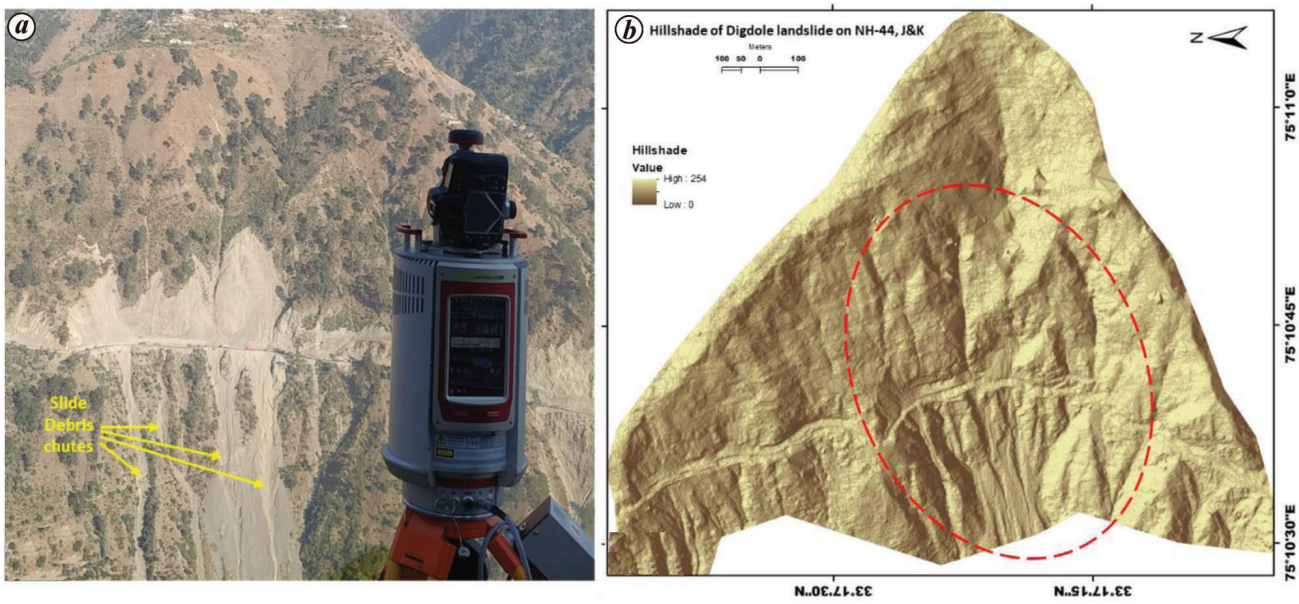

Figure 5. The case of extremely high point density enabling representation of micro-topography in the terrestrial lidar-generated DTM of Digdole landslide on NH-44, J&K. ***a***, Debris chutes downslope of NH-44 as seen from the opposite slope. ***b***, Micro-topographic details appreciably reflected in the generated DTM (inside the red oval).

over large inaccessible areas. The use of TLS in the site-specific study of all 15 landslides was driven by the need to produce rapid contour basemaps. Table 1 presents the minimum time spent in field site for data acquisition (both TLS and GNSS). GNSS data observation was done in fast static mode (1 h duration) at each of the identified GCPs for registration of the point cloud and a minimum of four GCPs/target reflectors for each study site to accommodate survey errors in the highly dissected Himalayan terrain. The relatively short time required for data acquisition in all the 15 sites indicates the efficiency over conventional survey methods.

From the 3D point cloud acquired by high-frequency scanning, a bare ground lidar dataset of each study site was prepared by separating the off-terrain points from terrain points using available terrain filters (Figure 4). This ability to generate a bare earth/terrain model by removing vegetation cover is a testament to the superiority of the technology over conventional survey methods. This unique advantage of the lidar-derived terrain model can provide information on the topographical and morphological changes in a landslide that may otherwise stay hidden beneath the vegetation cover in conventional surveys. High-density point cloud also allows for observation of very fine/minute details of the topography (Figure 5), which is essential for accurate slope characterization. Figure 6 reflects the significance of the acquired point data density vis-à-vis the quality of output data and the disadvantage of conventional surveys in tough terrain.

An incomparable advantage of the terrestrial lidar data in topographic surveys, particularly in the rapid hazard assessment of landslides, is the direct use of the point cloud for feature identification which hitherto is not available in conventional topographic surveys. Figure 7 *a* and *b* shows the use of the point cloud on a reflectance scale for the digitization of roads and rivers. Figure 7 *c* and *d* presents the true-colour point cloud (camera-captured), which allows for clarity and enhanced visualization for defining landslide boundaries and their attributes, more so in mapping over inaccessible and hazardous slopes.

Quality and utility of static terrestrial lidar output data in rapid hazard assessment of landslides

In the present study, the refined point cloud for each landslide site was exported as LAS dataset (open, binary file format for interchange and archiving of lidar data) to ArcGIS, where the point cloud was gridded using the linear interpolation technique to a 0.5 m grid DEM. Figures 8 and 9 present the HRDEM-derived slope and contour basemap for all the 15 test sites.

Terrestrial lidar measurements are subject to noise/errors induced by different factors, which can be instrumental, environmental, methodological or a combination (gross errors). The laser scanner accuracy is usually lower in field practice due to terrain complexity[28,29], high incident angles during scanning[30], nature of the reflecting surfaces[31], weather conditions at the time of scanning[32,33], vegetation cover[34,35], etc., thereby influencing the accuracy of DEM. Removal of vegetation is a major factor in laser scanning, the output of which heavily influences the quality of the DEM[36]. In addition, methodological errors arising during co-registration of multiple scans, choice of interpolation

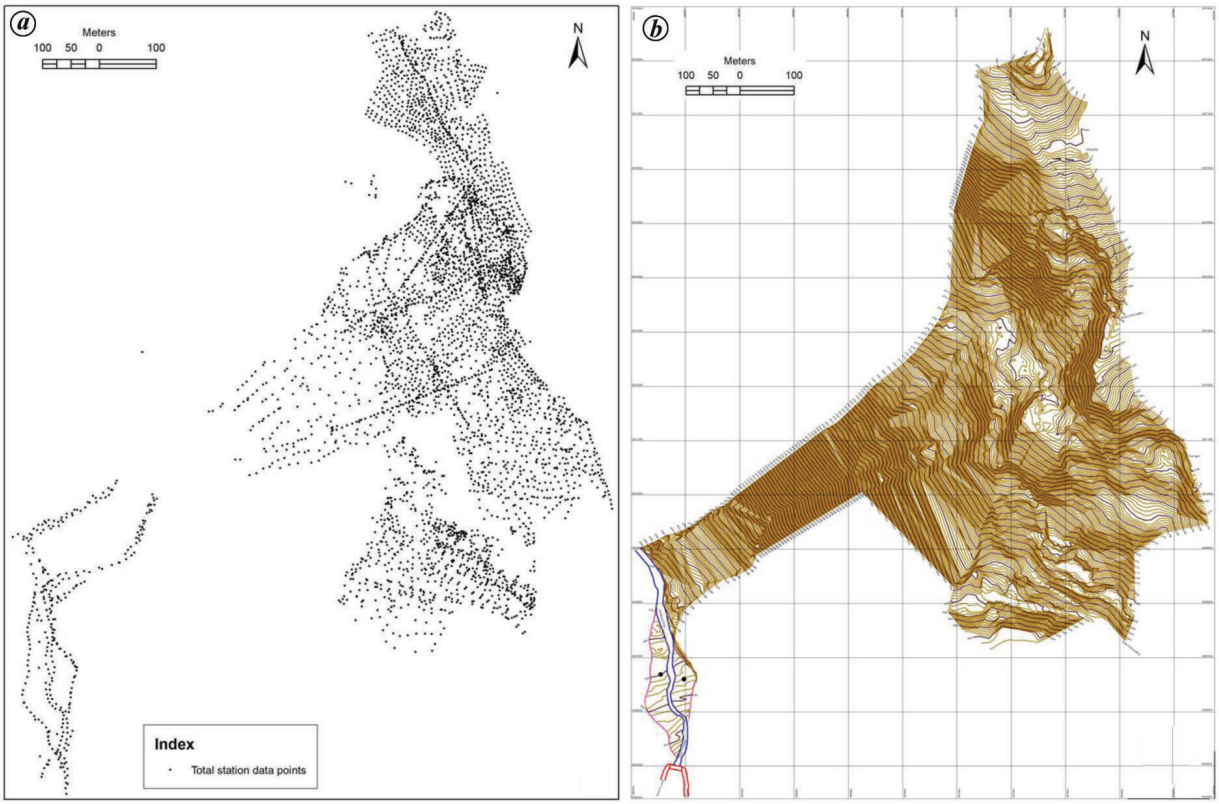

Figure 6. Total station (TS) survey for preparation of topographic basemap in the detailed study of the Tawang Monastery landslide, Arunachal Pradesh[43]: ***a***, Spatial distribution of TS point data (4,557), spread over an area of 0.48 km^2 and acquired during a timeframe of 10–11 days (November 2013). ***b***, The resultant errors (topography flattening) due to the lack of/lean point density is visible in the output contour basemap.

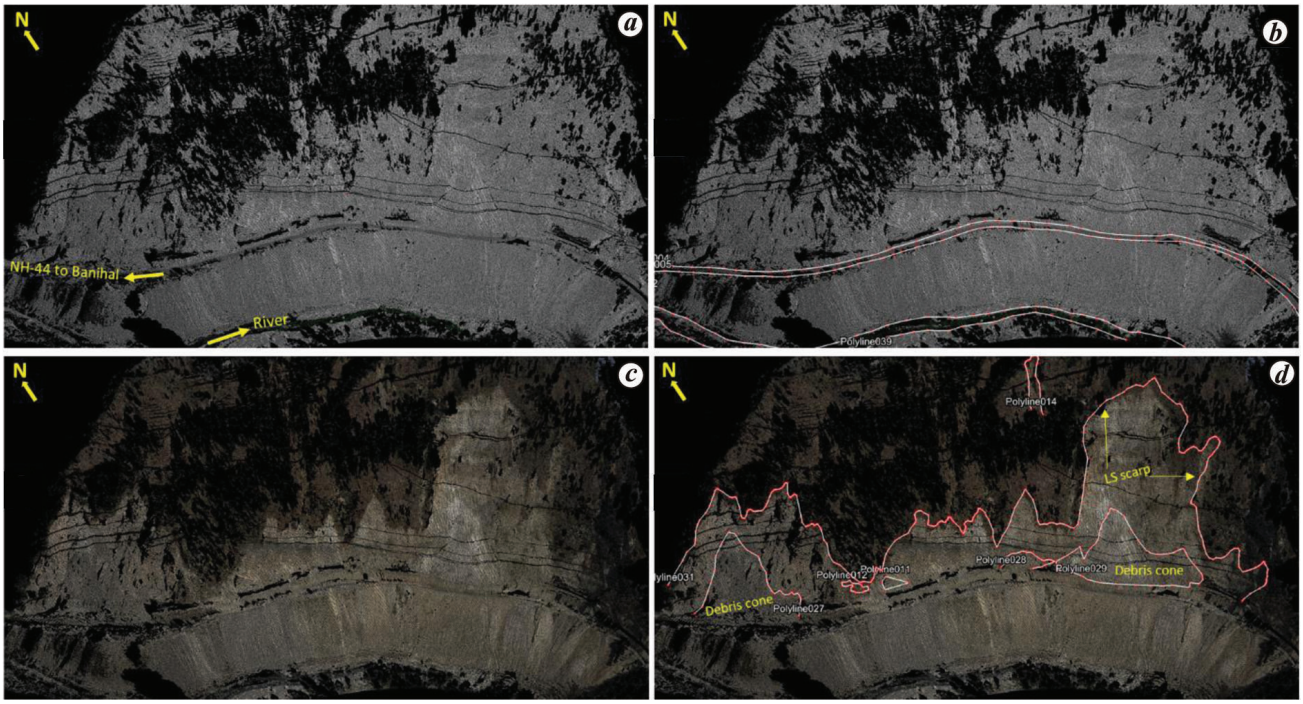

Figure 7. The refined point cloud for Monpassi landslide on NH-44, J&K. ***a***, Point cloud in reflectance scale. ***b***, Digitization of road and river based on reflectance contrast. ***c***, Point cloud in true colour (note the difference in visual information). ***d***, Mapping of landslide scarps and other visible attributes over inaccessible slopes.

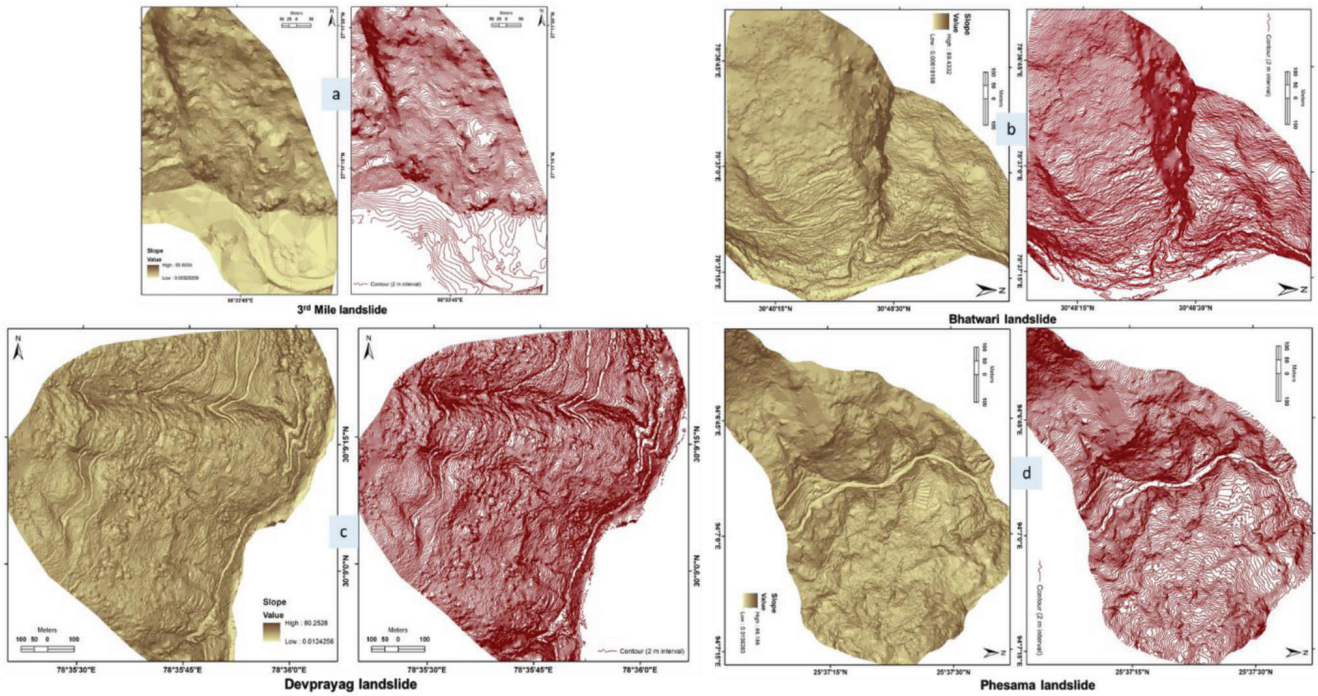

Figure 8. HRDEM-derived slope and contour basemaps of four study sites (some maps are orientated according to normal view of slopes for better visualization). ***a***, Third Mile landslide, Sikkim; ***b***, Bhatwari landslide, Uttarakhand; ***c***, Devprayag landslide, Uttarakhand; ***d***, Phesama landslide, Nagaland.

method in the development of DEM/DTM[37,38], etc. are also known to affect the accuracy of the output data. Buckley *et al.*[39] revealed the expected source of errors in a laser scanner workflow and the error budget for a long-range laser scanner. Under the circumstances, some amount of quality control measures verifying the accuracy of the output data (DEM/DTM) is crucial because errors in the base data will propagate through their derivative products (slope, aspect, curvature, contours) to be used for spatial analyses in site-specific landslide studies. In the present study, the quality of the generated HRDEM was checked following the most common DEM-error assessment method through computation of root-mean-square error (RMSE)[40,41] and mean error. The DEM elevation extracted in ArcGIS was spatially overlapped with the corresponding data of higher accuracy to highlight the errors (positive or negative) in the model. The more accurate (reference) data used was the independently acquired differential global positioning system (DGPS) data in real-time kinematic (RTK) mode. RTK data in the stop-and-go technique was collected over randomly distributed locations for the selected study sites. Calculating the mean error has shown overestimation in four and underestimation in three cases of the true ground elevations by DEM, the reason/s for inconsistency is not clearly understood in the present study. The RMSE calculated the following eq. (1) for the seven tested landslide sites is presented in Table 2, and shows a value ranging from 0.14 to 0.58 m.

$$\mathrm{RMSE} = \sqrt{[\Sigma(P_i - O_i)^2 / n]}, \tag{1}$$

where P_i the predicted/DEM-extracted value for the ith point in the elevation dataset, O_i the observed/reference value for the ith point in the elevation dataset and n is the sample size/count.

In addition to the primary task of preparing time-bound topographic basemaps required for the rapid hazard assessment, the by-products/derivatives (hillshade, slope and aspect) of the HRDEMs generated for the 15 landslides were directly used as support data for qualitative surface characterization and for mapping the geomorphologic attributes of the landslides. Through visual image analysis, the landslide morphological features such as the main scarp and flanks (landslide boundaries), zone of depletion and zone of accumulation were identifiable (expert judgement-based) using a slope/hillshade map derived from HRDEM (Figures 10 and 11). Critical information expected from the rapid assessment of landslides is the identification of unstable slopes and demarcation of potential areas/limits of the slopes for landslide retrogression/widening for adopting immediate action for risk reduction. Figure 12 illustrates a case where the synoptic 3D view obtained from the hillshade map has been upscaled through an overlay of the contour basemap on the aspect map for defining the maximum possible limits (slope facets) of the Marog1 landslide in the event of retrogression and/or widening.

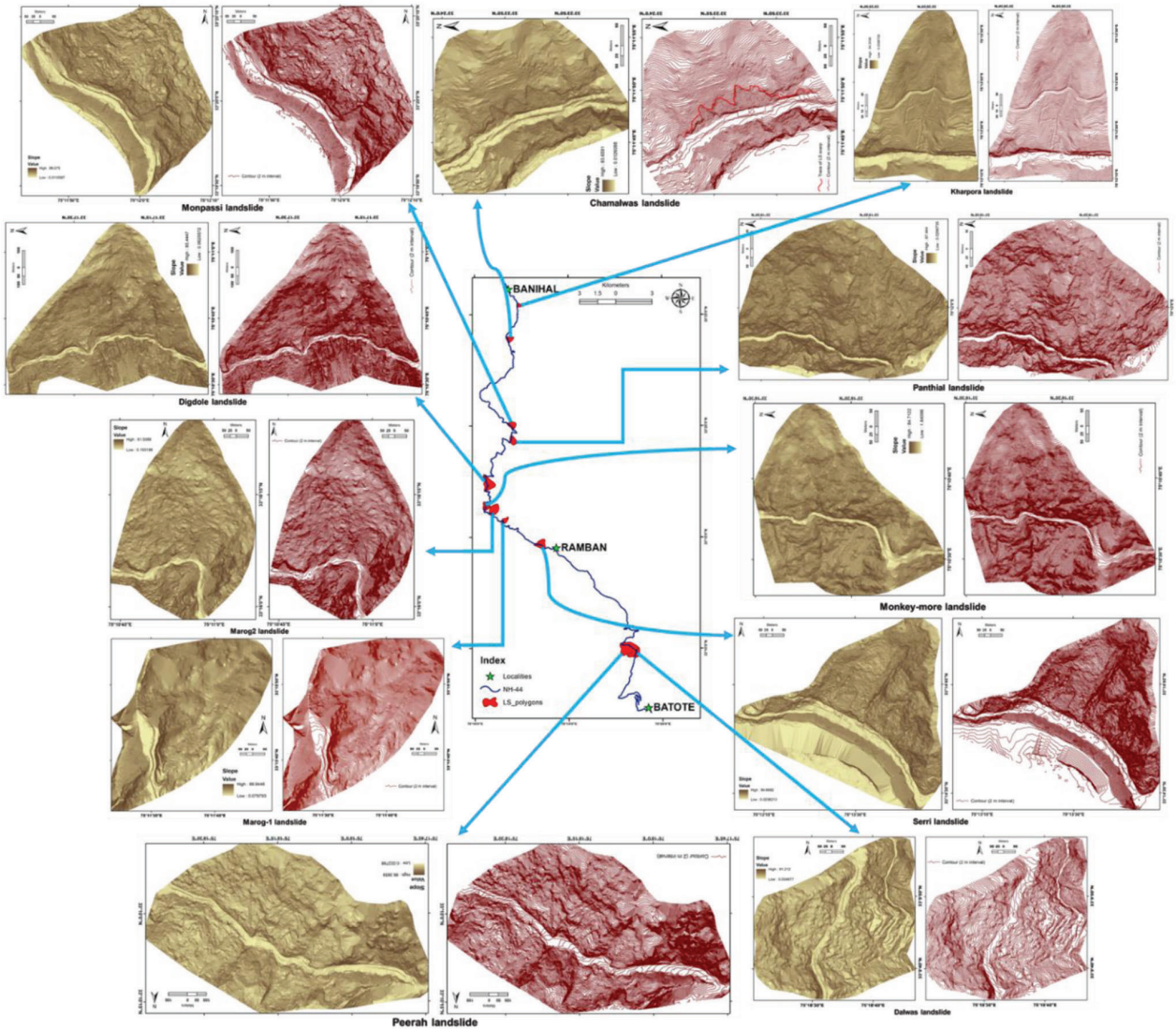

Figure 9. HRDEM-derived slope and contour basemap of the 11 landslides along Batote–Ramban–Banihal sector of NH-44, Jammu & Kashmir (some maps are orientated according to normal view of slopes for better visualization).

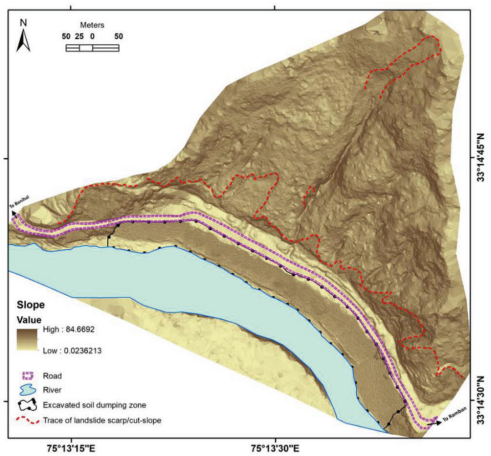

Figure 10. Visual-based mapping of landslide/cut-slope attributes using a slope map and supported by field verification (Serri landslide on NH-44, J&K).

Another feature aiding rapid assessment/characterization of landslides through the use of HRDEM and its derivatives is the quick preparation of slope profiles that are often used for understanding the geometry of failure surfaces (Figure 13) and in the preparation of 2D geological sections. The above-stated utilities drawn from the terrestrial lidar-derived HRDEM and its derivative products have been aptly used in the quick assessment of landslide characteristics and its geometry in the present study.

Discussion

The rapid hazard assessment of 15 landslides in the rugged Himalayan terrain, carried out through a TLS campaign, has revealed the superiority of static terrestrial lidars in generating basemaps for site-specific landslide studies. The unmatched advantages in terms of time invested for the

Table 2. Error statistics (m) from the accuracy assessment of digital elevation models for seven landslide sites

Site/location	No. of reference points used/sample size	Mean error	RMSE
3rd Mile landslide, Sikkim	20	0.2684	0.4849
Devprayag landslide, Uttarakhand	96	0.0252	0.1816
Dalwas landslide, J&K	07	–0.4253	0.5815
Digdole landslide, J&K	11	0.2981	0.5058
Monpassi landslide, J&K	12	–0.0124	0.4267
Peerah landslide, J&K	60	0.0143	0.1401
Phesama landslide, Nagaland	42	–0.2174	0.4141

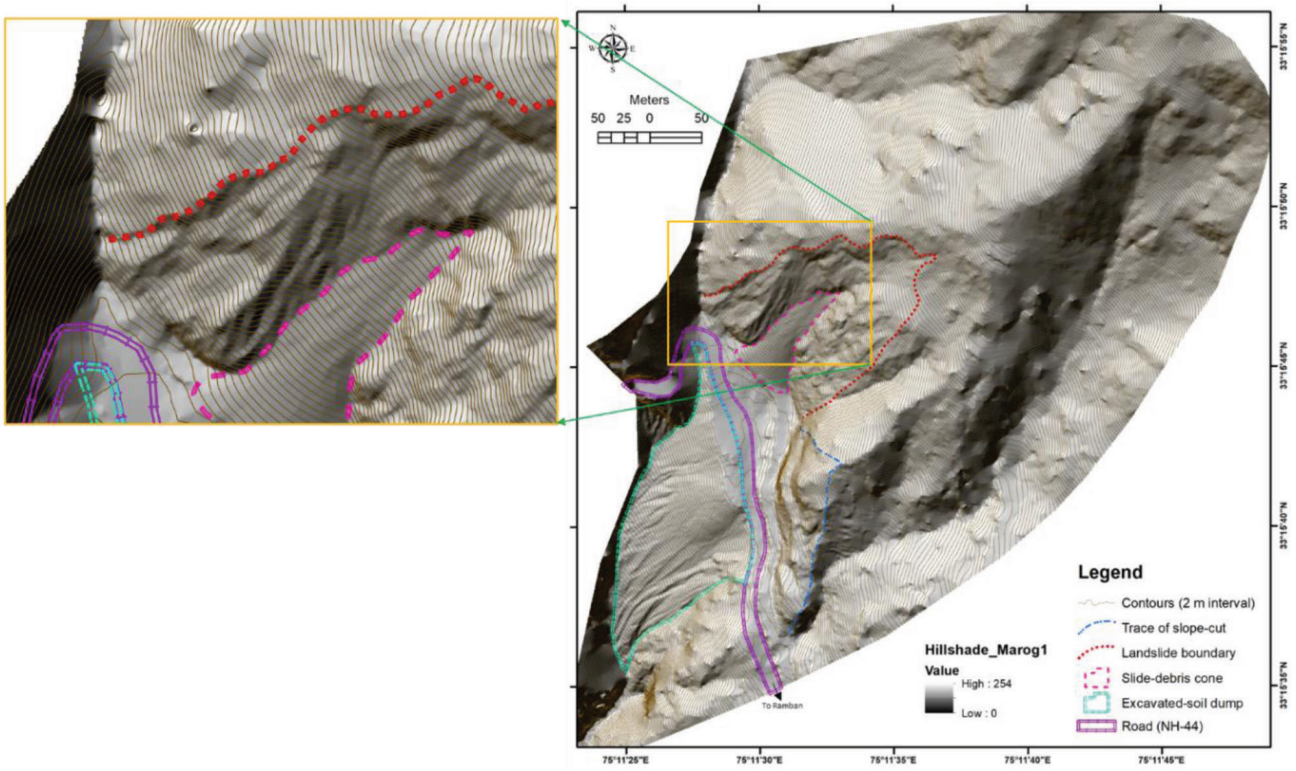

Figure 11. Surface characterization of the Marog1 landslide on NH-44, J&K through visual delineation and mapping of the landslide attributes. The contour basemap is superimposed on the hillshade map for optimal visualization.

acquisition of immensely dense 3D data have been explicitly demonstrated and the ensuing output qualifies for use in an emergency that necessitates a rapid DEM acquisition for assessing a landslide hazard. Further, the ability to penetrate vegetation cover enables the generation of a terrain model rather than a surface model, made possible through a virtual deforestation exercise by software-based removal of off-terrain points. The photographic information made available in the 3D point cloud enables mapping over inaccessible slopes and allows safe working conditions on hazardous slopes in a landslide. Exploiting such state-of-the-art devices and their high-quality output will help improve our understanding of landslide mechanisms and their processes in the rugged, landslide-prone Himalayan terrain.

The RMSE value obtained from the seven landslide DEMs was commensurate to the adopted cell size/resolution (0.5 m) of the generated DEM. Considering the nature of the task which is the extremely quick/time-bound generation of topographic basemaps required in the rapid hazard assessment of landslides, the complex Himalayan terrain with inherent practical difficulties and vegetation cover, a sufficiently accurate output DEM meeting the project requirements has been obtained using the terrestrial lidar. This is significant as the accuracy of the ensuing models on hazard assessment and stability analysis will largely depend on the exactness of the topography in the base model.

The seamless application of the terrestrial lidar in rugged terrain like the Himalayas is often constrained/restricted by lack of suitable scan positions due to limited accessibility

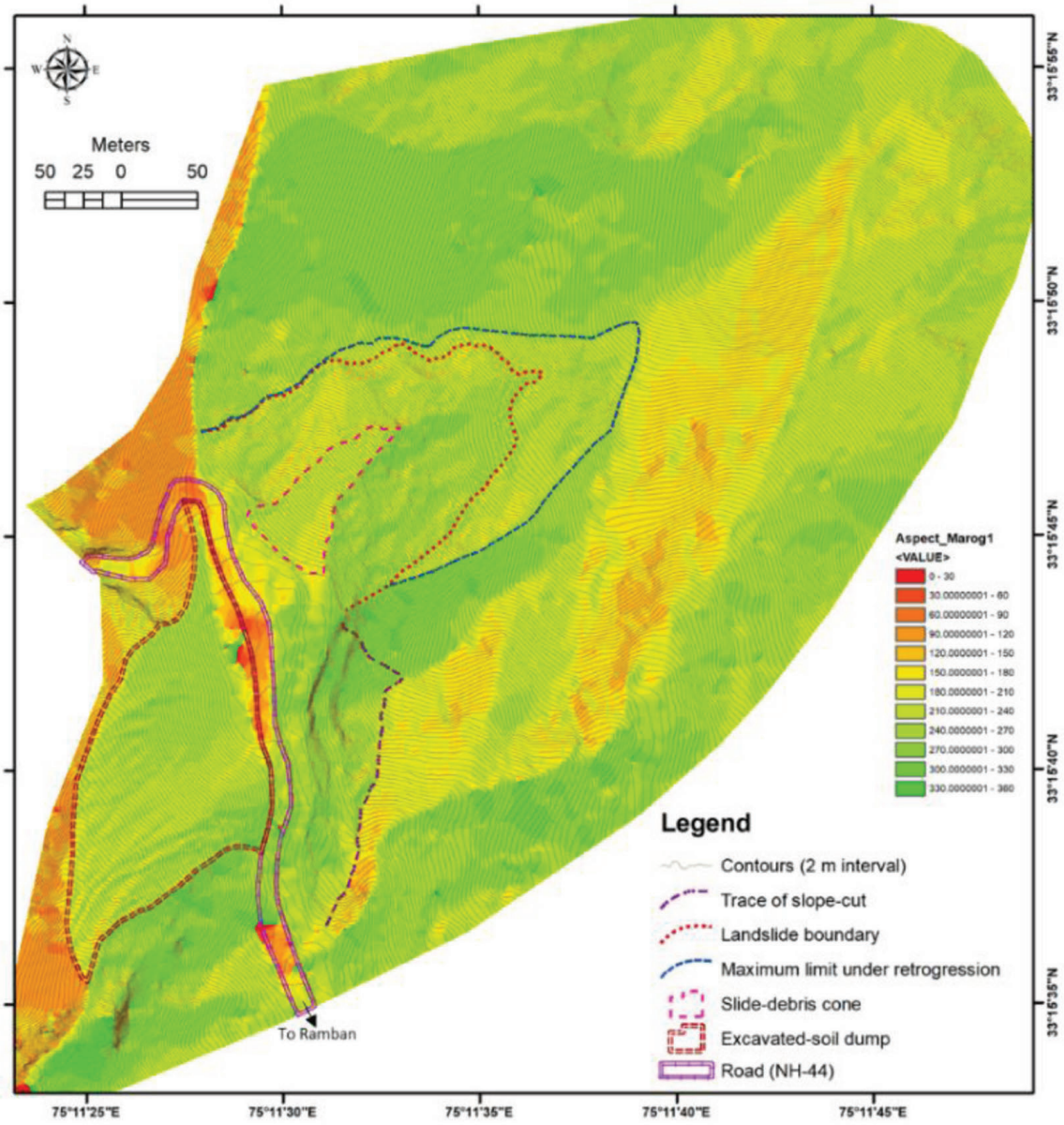

Figure 12. Demarcation of maximum possible landslide boundaries in the event of retrogression and/or widening, crucial for identification of the elements-at-risk.

conditions on the opposite slope, the complex slope morphometry giving rise to shadow areas and location of study sites within the effective scanning range of the instrument used. The case for lack of suitable scan positions in the present study is reflected in Table 1, where only a single station observation/scan was feasible for three study sites. While the data outputs in the present study have satisfactorily met the project requirements, it is clear that the challenges lie in improving the quality and accuracy of the output DEM, especially for higher accuracy studies like landslide monitoring through change detection. Other important domains on the use of terrestrial lidar in landslide studies not discussed here are the use of the acquired point cloud for characterization of discontinuities in rockslides and the generation of multi-temporal DEMs through repeat surveys for change detection that will remain the scope of future work.

Conclusion

The case for adoption and exploitation of the GNSS-supported TLS in site-specific landslide studies by the geoscientific community is supported by the outcome of the present study. The site-specific mapping of landslides made possible through the direct use of the point cloud, HRDEM and its derivatives has been aptly shown to effectively facilitate the rapid characterization of landslides which will

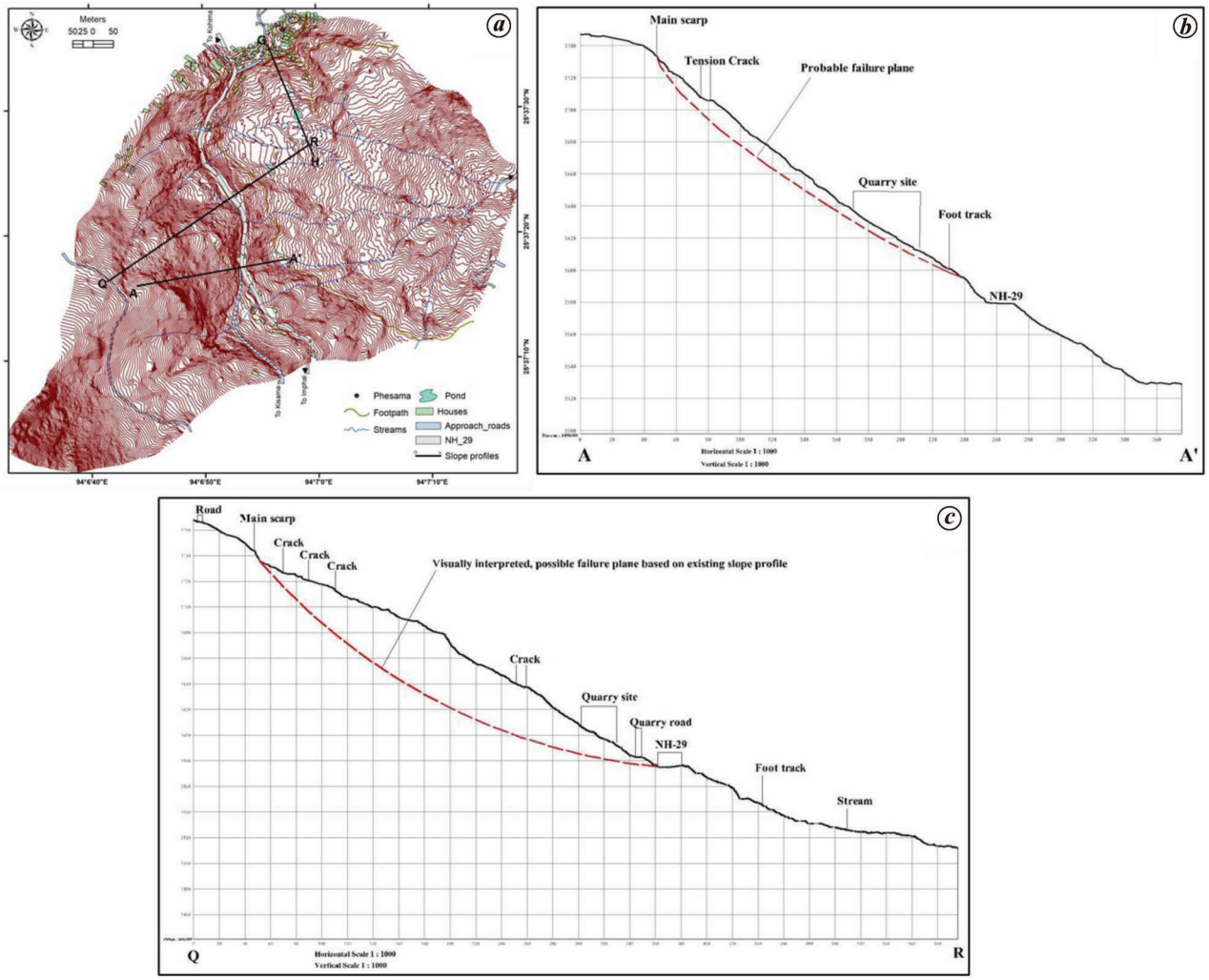

Figure 13. Two slope profiles of Phesama landslide, Nagaland prepared for interpretation on the geometry of failure surfaces. ***a***, Contour basemap of Phesama landslide showing the alignment of slope profiles. ***b***, Slope profile along *AA′* line showing the interpreted failure plane. ***c***, Slope profile along line *QR* showing the interpreted geometry of the failure plane.

go a long way towards adopting appropriate mitigation strategies within the shortest possible time for meaningful risk reduction. While the cost of lidar instruments and the associated software packages is high, the novel landslide mapping techniques offered by the static terrestrial lidar can revolutionize the rapid hazard assessment strategies in the hilly terrains, particularly for emerging disastrous landslides along road corridors and settlement areas.

1. Kvamme, K. L., Ernenwein, E. G. and Markussen, C. J., Robotic total station for microtopographic mapping: an example from the Northern Great Plains. *Archaeol. Prospect*., 2006, **13**, 91–102; doi: 10.1002/arp.270.
2. Schneider, T. D. and Panich, L. M., Total station mapping: practical examples from Alta and Baja California. *J. Calif. Great Basin Anthropol.*, 2008, **28**(2), 166–183.
3. McCaffrey, K. J. W. *et al.*, Unlocking the spatial dimension: digital technologies and the future of geoscience fieldwork. *J. Geol. Soc. London*, 2005, **162**, 927–938.
4. Jaboyedoff, M., Oppikofer, T., Abellán, A., Derron, M. H., Loye, A., Metzger, R. and Pedrazzini, A., Use of LIDAR in landslide investigations: a review. *Nat. Hazards*, 2012, **61**(1), 5–28; https://doi.org/10.1007/s1106 9-010-9634-2.
5. Abellan, A., Derron, Marc-Henri and Jaboyedoff, M., Use of 3D point clouds in geohazards. *Remote Sensing*, 2016, **8**, 130; doi: 10.3390/rs8020130.
6. Haneberg, W. C., Cole, W. F. and Kasali, G., High-resolution lidar-based landslide hazard mapping and modeling, UCSF Parnassus Campus; San Francisco, USA. *Bull. Eng. Geol. Environ.*, 2009, **68**, 263–276; doi:10.1007/s10064-009-0204-3.
7. Dunning, S. A., Massey, C. I. and Rosser, N. J., Structural and geomorphological features of landslides in the Bhutan Himalaya derived from terrestrial laser scanning. *Geomorphology*, 2009, **103**, 17–29; doi:10.1016/j.geomorph.2008.04.013.
8. Derron, M. H. and Jaboyedoff, M., LIDAR and DEM techniques for landslides monitoring and characterization. *Nat. Hazards Earth Syst. Sci*., 2010, **10**, 1877–1879.
9. Oppikofer, T. *et al.*, Investigation and monitoring of rock slope instabilities in Norway by terrestrial laser scanning. In *Landslides and Engineered Slopes: Protecting Society through Improved Understanding* (eds Eberhardt *et al.*), Taylor & Francis Group, London, UK, 2012, pp. 1235–1241; ISBN 978-0-415-62123-6.

10. Pawłuszek, K., Landslide features identification and morphology investigation using high-resolution DEM derivatives. *Nat. Hazards*, 2018; https://doi.org/10.1007/s11069-018-3543-1.
11. Gordon, S., Lichti, D. and Stewart, M., Application of a high-resolution, ground-based laser scanner for deformation measurements. In Proceedings of the 10th International FIG Symposium on Deformation Measurements, Orange, California, USA, 19–22 March 2001, pp. 23–32.
12. Chen, R. F., Chang, K. J., Angelier, J., Chan, Y. C., Deffontaines, B., Lee, C. T. and Lin, M. L., Topographical changes revealed by high-resolution airborne LiDAR data: the 1999 Tsaoling landslide induced by the Chi-Chi earthquake. *Eng. Geol.*, **88**, 160–172; doi:10.1016/j.enggeo.2006.09.008.
13. Corsini, A., Borgatti, L., Coren, F. and Vellico, M., Use of multitemporal airborne LiDAR surveys to analyse post-failure behaviour of earthslides. *Can. J. Remote Sensing*, 2007, **33**(2), 116–120.
14. Jaboyedoff, M. *et al.*, Use of terrestrial laser scanning for the characterization of retrogressive landslides in sensitive clay and rotational landslides in river banks. *Can. Geotech. J.*, 2009, **46**, 1379–1390.
15. Abellan, A., Jaboyedoff, M., Oppikofer, T. and Vilaplana, J. M., Detection of millimetric deformation using a terrestrial laser scanner: experiment and application to rockfall event. *Nat. Hazards Earth Syst. Sci*., 2009, **9**, 365–372; doi:10.5194/nhess-9-365-2009.
16. Rosser, N. J., Petley, D. N., Lim, M., Dunning, S. A. and Allison, R. J., Terrestrial laser scanning for monitoring the process of hard rock coastal cliff erosion. *Q. J. Eng. Geol.*, 2005, **38**(4), 363–375; doi:10.1144/1470-9236/05-008.
17. Travelletti, J., Oppikofer, T., Delacourt, C., Malet. J.-P. and Jaboyedoff, M., Monitoring landslide displacements during a controlled rain experiment using a long-range terrestrial laser scanning (TLS). *Int. Arch. Photogramm. Remote Sensing*, 2008, **37**(B5), 485–490.
18. Baldo, M., Bicocchi, C., Chiocchini, U., Giordan, D. and Lollino, G., LiDAR monitoring of mass wasting processes: the Radicofani landslide, Province of Siena, Central Italy. *Geomorphology*, 2008, **105**, 193–201; doi:10.1016/j.geomorph.2008.09.015.
19. Slob, S., van Knapen, B., Hack, R., Turner, K. and Kemeny, J., Method for automated discontinuity analysis of rock slopes with three-dimensional laser scanning. *Transp. Res. Rec.: J. Trans. Res. Board*, 2005, **1913**(1), 187–194; doi:10.1177/0361198105191300118.
20. Olariu, M. I., Ferguson, J. F. and Aiken, C. L. V., Outcrop fracture characterization using terrestrial laser scanners: deepwater jackfork sandstone at Big Rock Quarry, Arkansas. *Geosphere*, 2008, **4**(1), 247–259; doi:10.1130/GES00139.1.
21. Lato, M., Diederichs, M. S., Hutchinson, D. J. and Harrap, R., Optimization of lidar scanning and processing for automated structural evaluation of discontinuities in rockmasses. *Int. J. Rock Mech. Min. Sci*., 2009, **46**, 194–199; doi:10.1016/j.ijrmms.2008.04.007.
22. Sturzenegger, M. and Stead, D., Close-range terrestrial digital photogrammetry and terrestrial laser scanning for discontinuity characterization on rock cuts. *Eng. Geol*., 2009, **106**, 163–182; doi:10.1016/j.enggeo.2009.03.004.
23. Gigli, G. and Casagli, N., Semi-automatic extraction of rock mass structural data from high resolution LiDAR point clouds. *Int. J. Rock Mech. Min. Sci.*, 2011, **48**(2), 187–198; doi:10.1016/j.ijrmms.2010.11.009.
24. Wehr, A. and Lohr, U., Airborne laser scanning – an introduction and overview. *ISPRS J. Photogramm. Remote Sensing*, 1999, **54**(2–3), 68–82; doi:10.1016/s0924-2716(99)00011-8.
25. Petrie, G. and Toth, C. K., I. Introduction to laser ranging, profiling and scanning, II. Terrestrial laser scanners. In *Topographic Laser Ranging and Scanning: Principles and Processing* (eds Shan, J. and Toth, C. K.), CRC Press, Taylor & Francis, 2008, 2nd edn, pp. 1–6.
26. RIEGL Laser Measurement Systems GmbH, RIEGL VZ-4000 data sheet, 2017; www.riegl.com
27. Abd-Elmaaboud, A. M., El-Tokhey, M. E., Ragheb, A. E. and Mogahed, Y. M., Comparative assessment of terrestrial laser scanner against traditional surveying methods. *Int. J. Eng. Appl. Sci.*, 2019, **6**(4), 79–84.
28. Fan, L. and Atkinson, P. M., Accuracy of digital elevation models derived from terrestrial laser scanning data. *IEEE Geosci. Remote Sensing Lett.*, 2015, **12**(9), 1923–1927.
29. Su, J. and Bork, E., Influence of vegetation, slope and lidar sampling angle on DEM accuracy. *Photogramm. Eng. Remote Sensing*, 2006, **72**(11), 1265–1274.
30. Soudarissanane, S., Lindenbergh, R., Menenti, M. and Teunissen, P., Incidence angle influence on the quality of terrestrial laser scanning points. In Proceedings of the ISPRS Workshop on Laser Scanning, Paris, France, 1–2 September 2009, p. 38.
31. Voegtle, T., Schwab, I. and Landes, T., Influences of different materials on the measurement of a terrestrial laser scanner (TLS). In Proceedings of the XXI Congress, International Society for Photogrammetry and Remote Sensing, Beijing, 2008, pp. 1061–1066.
32. Rasshofer, R., Spies, M. and Spies, H., Influences of weather phenomena on automotive laser radar systems. *Adv. Radio Sci.*, 2011, **9**, 49–60; doi:9.10.5194/ars-9-49-2011.
33. Hejbudzka, K., Lindenbergh, R., Soudarissanane, S. and Humme, A., Influence of atmospheric conditions on the range distance and number of returned points in Leica ScanStation 2 point clouds. *Int. Arch. Photogramm., Remote Sensing Spat. Inf. Sci.*, 2010, **XXXVIII**, 282–287.
34. Spaete, L., Glenn, N., Derryberry, D., Sankey, T., Mitchell, J. and Hardegree, S., Vegetation and slope effects on accuracy of a LIDAR-derived DEM in the sagebrush steppe. *Remote Sensing Lett*., 2011, **2**, 317–326; 10.1080/01431161.2010.515267.
35. Pfeifer, N., Gorte, B. and Oude, E. S., Influences of vegetation on laser altimetry – analysis and correction approaches. *Int. Arch. Photogramm., Remote Sensing Spat. Inf. Sci.*, 2012, **36**.
36. Harding, D., Pulsed laser altimeter ranging techniques and implications for terrain mapping. In *Topographic Laser Ranging and Scanning: Principles and Processing* (eds Shan, J. and Toth, C. K.), CRC Press, Taylor & Francis, 2008, pp. 173–194.
37. Heritage, G. L., Milan, D. J., Large, A. R. G. and Fuller, I. C., Influence of survey strategy and interpolation model on DEM quality. *Geomorphology*, 2009, **112**(3/4), 334–344.
38. Erdogan, S., A comparison of interpolation methods for producing digital elevation models at the field scale. *Earth Surf. Process. Landf.*, 2009, **34**(3), 366–376.
39. Buckley, S. J., Howell, J. A., Enge, H. D. and Kurz, T. H., Terrestrial laser scanning in geology: data acquisition, processing and accuracy considerations. *J. Geol. Soc., London*, 2008, **165**, 625–638.
40. Hunter, G. J. and Goodchild, M. F., Modeling uncertainty of slope and aspect estimates derived from spatial databases. *Geogr. Anal*., 1997, **29**(1), 35–49.
41. Aquilar, F. J., Aguera, F., Aquilar, M. A. and Carvajal, F., Effects of terrain morphology, sampling density and interpolation methods on grid DEM accuracy. *Photogramm. Eng. Remote Sensing*, 2005, **71**(7), 805–816.
42. SoI, Political map of India, English 10th edition, Survey of India, Government of India, 2020; https://surveyofindia.gov.in/documents/polmap-eng-11012021.jpg
43. Chasie, M., Theophilus, P. K., Chakraborty, D. and Sarkar, N. K., Detailed geotechnical evaluation of the Tawang Monastery landslide, Arunachal Pradesh. *Indian J. Geosci.*, 2017, **71**(4), 627–634.

ACKNOWLEDGEMENTS. This work has been carried out as part of the annual field season programme of the Geological Survey of India (GSI), Ministry of Mines, Government of India. We thank the Director General, GSI, Kolkata for permission to publish this paper. We also thank the anonymous reviewers for their comprehensive reviews and comments that helped improve this manuscript.

Received 29 March 2022; revised accepted 20 July 2022

doi: 10.18520/cs/v123/i7/844-855